Heavy boron doping in superconducting carbon materials

Yuki Sakai,[1] James R. Chelikowsky,[1,2,3] and Marvin L. Cohen[4,5]
[1]*Center for Computational Materials, Oden Institute for Computational Engineering and Sciences, The University of Texas at Austin, Austin, Texas 78712, USA*
[2]*McKetta Department of Chemical Engineering, The University of Texas at Austin, Austin, Texas 78712, USA*
[3]*Department of Physics, The University of Texas at Austin, Austin, Texas 78712, USA*
[4]*Department of Physics, University of California at Berkeley, Berkeley, California 94720, USA*
[5]*Materials Sciences Division, Lawrence Berkeley National Laboratory, Berkeley, California 94720, USA*

(Received 12 February 2020; accepted 14 April 2020; published 4 May 2020)

We examine physical properties of heavily boron-doped sp^3-hybridized carbon allotropes: cubic diamond, hexagonal diamond, and body centered tetragonal C_4. The structural similarity between cubic diamond and hexagonal diamond leads to similar responses to substitutional boron doping. On the other hand, body centered tetragonal C_4 exhibits distinct structural and electronic properties because of its characteristic structure. Our study also shows that the superconducting transition temperatures up to 60 K are possible in heavily doped carbon materials despite their various atomistic structures.

DOI: 10.1103/PhysRevMaterials.4.054801

I. INTRODUCTION

Carbon has various allotropes with different crystal structures. Graphite is composed of layers of sp^2-hybridized carbon atoms arranged into a honeycomb lattice. The single layer of graphite, two-dimensional graphene, has special properties which normal three-dimensional materials do not possess [1]. The carbon nanotube is a one-dimensional cylinder of graphene, which shows interesting electronic properties depending on its chirality [2,3]. The fullerene (C_{60}) molecule is another sp^2 allotrope of carbon, which forms a crystalline solid [4].

There are sp^3-hybridized carbon allotropes where atoms are fourfold coordinated. The most abundant sp^3 carbon allotrope is cubic diamond. Lonsdaleite, hexagonal diamond, is another sp^3 allotrope with a 2H or wurtzite-type structure if we view cubic diamond as a 3C (zinc-blende-type) structure. In addition to these existing materials, there are numerous computationally designed allotropes of carbon. For example, the carbon kagome lattice has a direct band gap owing to its characteristic orbital frustration and is promising for optical applications [5,6]. M-carbon, W-carbon, and body centered tetragonal C_4 (bct C_4) have been proposed to explain the carbon phase that appears when graphite is compressed at low temperature [7–10]. These existing and proposed carbon materials exhibit various interesting properties depending on their detailed atomistic structures.

Carbon materials become superconductors typically when carriers are doped. For instance, doping alkali atoms to the internal space of fullerene crystals and graphite yields superconductivity thorough electron doping [11,12]. The highest superconducting transition temperature (T_c) is 11.5 and 33 K for graphite (CaC_6) and fullerene ($Cs_xRb_yC_{60}$) cases, respectively. Boron (hole) doping in a carbon nanotube causes superconductivity with the highest T_c of 19 K under pressure [13,14]. The high T_c is believed to occur when the one-dimensional van Hove singularity in the density of states of a nanotube is aligned with the Fermi energy shifted by hole doping [14]. Boron-doped sp^3 cubic diamond exhibits superconductivity due to shallow acceptor states with a T_c up to 11 K [15–17]. Even when no carriers are doped, twisted bilayer graphene at "magic twist angles" exhibits superconductivity [18].

The recent finding of the high T_c of 55 K in heavily boron-doped amorphous "Q-carbon" motivates further investigations of high T_c in boron-doped carbon materials [19–22]. In particular, sp^3-hybridized carbon materials should be of interest as Q-carbon is considered to be an sp^3-rich material [23,24]. A potentially higher T_c associated with the high electronic density of states at the Fermi energy in heavily boron-doped cubic diamond was theoretically proposed by Moussa and Cohen [25]. However, the effect of heavy boron doping in other carbon allotropes has not been well studied. Understanding the superconductivity in boron-doped carbon materials with different crystal structures should also help understanding the interesting properties of Q-carbon since the detailed mechanism of the high-temperature superconductivity and the atomistic structure remains an open question.

Here we study the superconductivity in several different boron-doped sp^3 carbon allotropes. We select cubic diamond and hexagonal diamond because they are found in nature. We also consider bct C_4 since this material has characteristic four-membered rings in its structure, which are sometimes observed in amorphous carbon. We consider different concentrations of substitutionally doped boron atoms (12.5%, 25%, and 50%) to see their effect on physical properties. Hexagonal diamond exhibits similar properties to those of cubic diamond owing to their structural similarity even when doped with boron atoms. On the other hand, the characteristic structure of bct C_4 causes structural and electronic responses to boron doping that are different from cubic and hexagonal diamond. In spite of such distinct properties, even bct C_4

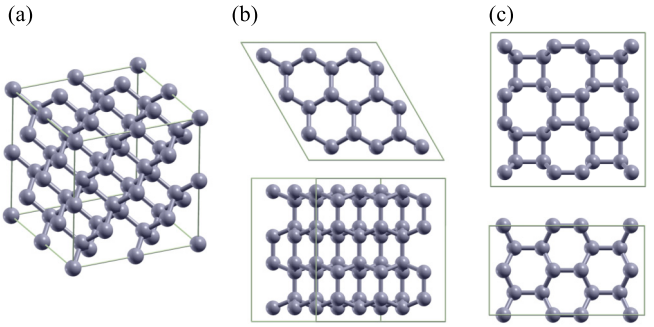

FIG. 1. Crystal structures of (a) cubic diamond, (b) hexagonal diamond, and (c) body centered tetragonal (bct) C_4. The top and bottom panels of (b) and (c) represent the top and side views of the structures, respectively. Carbon atoms are illustrated with gray spheres. The size of the cell is equivalent to the initial undoped supercell used in this work. The number of atoms is 64 in (a) and (c), while (b) contains 72 atoms.

exhibits similar superconducting properties to other carbon materials.

II. COMPUTATIONAL METHOD

We employ a total-energy pseudopotential method constructed within density functional theory (DFT) [26–29]. A plane-wave basis is used to represent wave functions with a cutoff energy of 65 Ry, respectively [30]. Troullier-Martins norm-conserving pseudopotentials are constructed by using local density approximation for the exchange-correlation energy functional [31–33].

Cubic and orthorhombic $2 \times 2 \times 2$ supercells containing 64 atoms are used for simulations of cubic diamond and bct C_4, respectively, as shown in Figs. 1(a) and 1(c). For hexagonal diamond, we use a $3 \times 3 \times 2$ supercell with 72 carbon atoms [see Fig. 1(b)]. A k grid of $2 \times 2 \times 2$ is used for the total-energy calculations and structural relaxations of cubic diamond. For hexagonal diamond and bct C_4, we use a $2 \times 2 \times 4$ k grid. We take a denser $8 \times 8 \times 8$ k grid for the calculation of electronic densities of states (DOS) with the tetrahedron method.

Density functional perturbation theory is used to simulate vibrational and superconducting properties [34]. Phonon calculations are performed with a $2 \times 2 \times 2$ k grid using Γ-only sampling in the phonon q space. The electron-phonon linewidth for each phonon mode is calculated from the electron-phonon matrix elements [35]. Here we use a finer $6 \times 6 \times 6$ k grid to obtain accurate results. A Gaussian broadening of 0.015–0.025 Ry is used to approximate the δ function that appears in the Brillouin-zone summations. We further compute the Eliashberg spectral function and electron-phonon coupling strength λ by using the linewidth obtained above. The superconducting transition temperature is estimated from the electron-phonon coupling strength λ by using the Allen-Dynes equation [36] with an effective Coulomb repulsion parameter μ^* of 0.12.

We focus on substitutional boron doping in this work as the contribution from boron interstitial doping to superconductivity is not significant [37]. We study 128 completely randomly substituted boron-doped structures for the boron concentration of 12.5%, 25%, and 50%. In addition to these random sets, we independently generate 48 structures without pairing (neighboring) of boron atoms for 25% boron-doping cases to consider the effect of boron pairing. We perform a variable-cell structural relaxation [38] for each structure after boron atoms are incorporated.

III. RESULTS AND DISCUSSION

We consider the effect of boron pairing on the energetic stability of boron-doped carbon materials. Table I lists the total-energy statistics of three 25% boron-doped allotropes. The effect of boron pairing on the average energy is relatively small in cubic diamond and hexagonal diamond (the energy differences are 0.1 and 0.3 eV/cell, respectively). The lowest-energy structure does not have the pairing in either case. These data show that the stability in terms of the total energy should not be strongly affected by the existence of boron pairing in these materials. On the other hand, the boron-pairing costs energy in bct C_4 by 0.7 eV/cell, on average. The highest energy of bct C_4 with boron pairing is 0.9 eV/cell higher than that without pairing. This indicates that boron pairing is not favored in bct C_4 when compared with other allotropes.

Heavy boron doping causes structural distortions even in relatively rigid cubic and hexagonal diamond. Figures 2(a) and 2(b) [Figs. 2(c) and 2(d)] illustrate the structure of 25% boron-doped cubic (hexagonal) diamond with and without boron pairing, respectively. The boron-boron bond tends to be longer than the carbon-carbon and carbon-boron bonds, as shown in Figs. 2(a) and 2(c). This tendency causes a strong structural distortion around clustered boron atoms. In fact, the structure without boron pairing [Figs. 2(b) and 2(d)] is almost the same as that of the undoped case shown in Figs. 1(a)

TABLE I. Total energies (in eV/cell) of boron-doped cubic diamond, hexagonal diamond, and bct C_4 with 25% boron concentration. The highest, lowest, and average total energies of randomly generated structures are listed. The left and right subcolumns for each material indicate structures with and without boron pairing (BP), respectively. The zero of the total energy is that of the lowest-energy structure for each allotrope.

	Cubic diamond		Hexagonal diamond		bct C_4	
	BP	no BP	BP	no BP	BP	no BP
Average	2.2	2.3	1.7	1.4	2.3	1.6
Highest	4.0	3.9	3.4	3.2	4.2	3.3
Lowest	0.8	0	0.05	0	0.4	0

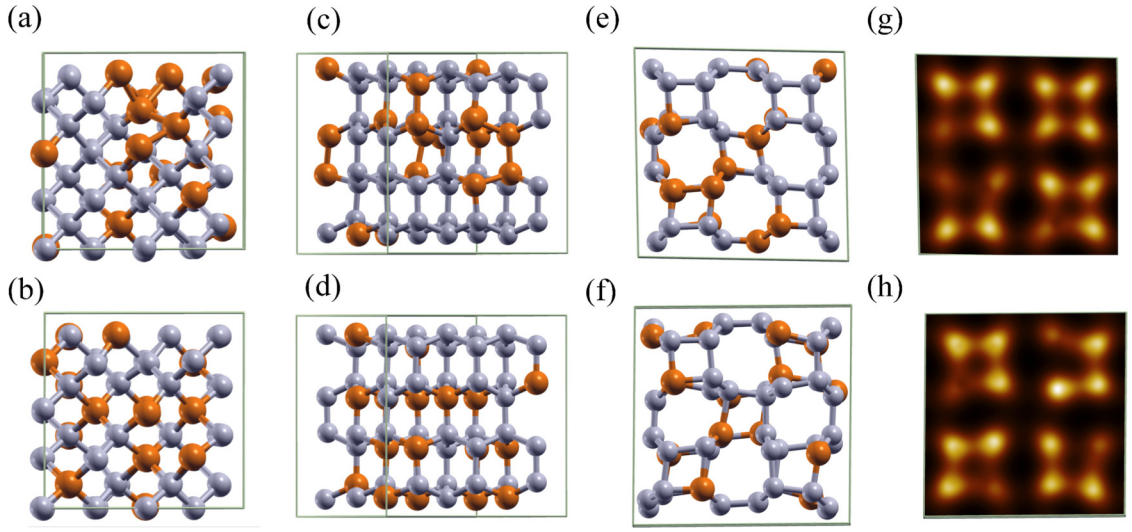

FIG. 2. Distorted crystals structure of 25% boron-doped carbon allotropes. The structure of cubic diamond, (a) with and (b) without boron pairing, hexagonal diamond (c) with and (d) without boron pairing, and bct C_4 (e) with and (f) without boron pairing. (a),(c),(e) The highest-energy structure among each set; (b),(d),(f) the lowest-energy structures. Gray and orange spheres represent carbon and boron atoms, respectively. (g) Charge density color plot taken at a plane right above the topmost atoms of (e). (h) Similar plot, but for (f). Here a black-brown-white color scale is used.

and 1(b). The distortion is more significant in bct C_4, as illustrated in Figs. 2(e) and 2(f). The bct C_4 is less stable than diamond, as indicated by the uneven bond angles (90, 111, or 114 degrees) deviated from the ideal sp^3 bond angle (109.5 degrees). For example, boron dopants strongly distort the square shape in Fig. 2(f).

The square-shaped four-membered rings formed by the 90 degrees bonds are more strongly distorted in bct C_4 when no boron pairing exists, as shown in Fig. 2(f). This is completely opposite from hexagonal diamond, where the boron pairing promotes stronger distortion. The boron-carbon bond length is 2.24 Å in the upper-right broken square. This indicates that these atoms are almost threefold coordinated (i.e., sp^2-hybridized). The charge density described in Fig. 2(h) confirms that no bonding is formed between the two atoms. Such a change in the coordination number cannot be observed in the case with boron pairing, as the charge density map in Fig. 2(g) shows. The boron-doped site favors threefold coordination because of the electron deficiency. However, a longer boron-boron bond length prevents the boron atoms from lowering the coordination number when the boron pairing exists. Here the average nearest-neighbor boron-boron bond length (1.77 Å) is longer by 0.2 Å than that of the structures without boron pairing (1.57 Å) when we take 2.0 Å as a threshold. The lower coordination number in boron-doped bct C_4 explains the relatively large energy difference (0.7 eV/cell) between those with and without boron pairing.

Boron pairing significantly affects the electronic properties as well. Figure 3 shows the partial electronic density of states (PDOS) of 25% boron-doped carbon allotropes. Here the left and right columns correspond to the structures with and without boron pairing, respectively. The electronic properties show a considerable difference, particularly around the Fermi energy. The PDOS for carbon and boron atoms is almost equivalent when there is no boron pairing because the dopant distribution can be regarded as uniform [see Figs. 3(b), 3(d), and 3(f)]. On the other hand, the boron PDOS is larger than that of carbon when boron pairing exists because of localized acceptor states created by the pairing or clustering of boron atoms. Figures 3(a), 3(c), and 3(e) clearly indicates that boron contributions shows high and localized PDOS, particularly around 2 eV above the Fermi energy.

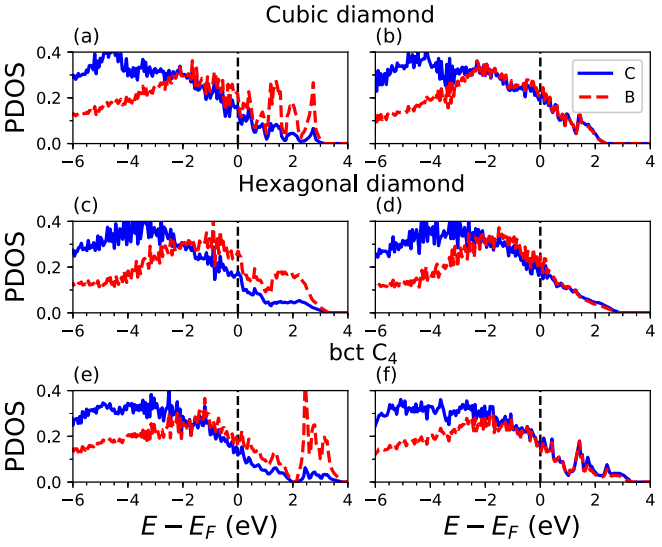

FIG. 3. Partial electronic DOS (PDOS) in states/eV/atom of (a),(b) cubic diamond, (c),(d) hexagonal diamond, and (e),(f) bct C_4. (a),(c),(e) The PDOS for the structures with boron pairing; (b),(d),(f) those without boron pairing. The boron concentration is 25% and the PDOS is the average over all atoms from each atomic species. Blue solid and red dashed lines represent the partial DOS of carbon and boron atoms, respectively. The vertical dashed line shows the position of the Fermi energy.

TABLE II. Electronic density of states at the Fermi energy [$N(E_F)$ in state/eV/atom] of boron-doped cubic diamond, hexagonal diamond, and bct C_4 with 12.5%, 25%, and 50% boron doping. Here the highest (MAX), lowest (MIN), and average (AVG) of $N(E_F)$ are listed. The left and right subcolumns for each material with 25% doping indicate structures with and without boron pairing (BP), respectively. We do not distinguish the existence of boron paring in the 12.5% and 50% doped cases.

		Cubic diamond		Hexagonal diamond		bct C_4	
		BP	no BP	BP	no BP	BP	no BP
	AVG	0.09		0.10		0.09	
12.5%	MAX	0.14		0.14		0.14	
	MIN	0.05		0.06		0.04	
	AVG	0.13	0.19	0.13	0.17	0.11	0.13
25%	MAX	0.18	0.26	0.18	0.21	0.16	0.18
	MIN	0.07	0.15	0.08	0.14	0.04	0.09
	AVG	0.12		0.12		0.13	
50%	MAX	0.17		0.16		0.17	
	MIN	0.04		0.07		0.05	

Table II lists the average, lowest, and highest electronic DOS at the Fermi energy [$N(E_F)$] of three carbon materials with different amount of boron doping. The increase in boron concentration from 12.5% to 25% contributes to the higher average $N(E_F)$ by 44, 30, and 11% for cubic diamond, hexagonal diamond, and bct C_4, respectively when boron pairing exists. The $N(E_F)$ is more than double in cubic diamond when boron pairing is avoided. This confirms that the localization of acceptor states caused by boron pairing prevents an increase in $N(E_F)$. In fact, even 50% boron doping does not increase both the average and highest $N(E_F)$ (0.12 and 0.17 states/eV/atom, respectively) in cubic diamond because of inevitable boron paring in heavy boron doping. Also, $N(E_F)$ does not increase in hexagonal diamond and bct C_4 in a similar fashion even with 50% doping.

The average and the highest $N(E_F)$ of bct C_4 is almost the same as those of cubic diamond and hexagonal diamond when the boron concentration is 12.5%. However, the average $N(E_F)$ without boron pairing is smaller by 32% and 24% when compared with cubic and hexagonal diamond, respectively. This indicates that the increase in the $N(E_F)$ with respect to boron concentration is slower than in the other allotropes. In addition, cubic and hexagonal diamond does not exhibit clear localization of electronic states above the Fermi energy, while the localized states are prominent in the PDOS of bct C_4 [see Figs. 3(b), 3(d), and 3(f)]. Boron doping causes a large structural distortion in bct C_4. We see that some atoms are threefold coordinated, as illustrated in Fig. 2(d). Such sp^2-like atoms have remaining p_z orbitals, which are not used for bonding. These remaining orbitals appear within the band gap and form localized states in a similar fashion to dense amorphous carbon [20,24]. The structural distortion due to boron doping causes the distinct electronic properties of bct C_4.

Figure 4 displays the superconducting temperature (T_c), the logarithmic average of phonon frequency ($\omega_{\log}$), and the electron-phonon coupling constant (λ) as a function of $N(E_F)$ for boron-doped carbon allotropes. Here we select samples from a set of randomly doped structures as follows: three structures with high $N(E_F)$, three with low $N(E_F)$, and three with $N(E_F)$ close to the average $N(E_F)$ for each boron-doping concentration and material. For those without boron pairing, we take three structures with high $N(E_F)$ and compute superconducting properties. We obtain the highest T_c of 57, 47, and 55 K for cubic diamond, hexagonal diamond, and bct C_4, respectively.

The almost linear correlation between $N(E_F)$ and λ is observed in all three carbon allotropes in Fig. 4. On the other hand, the $\omega_{\log}$ is weakly but negatively correlated with $N(E_F)$. The reduction of $\omega_{\log}$ occurs because of the weakened chemical bonds owing to the increase of the number of boron atoms. The respective clustering of blue squares (12.5% doped cases) and green circles (25% doped cases) shows this relation between the doping concentration and $\omega_{\log}$. T_c exhibits a similar trend to λ, although the linear correlation is relatively

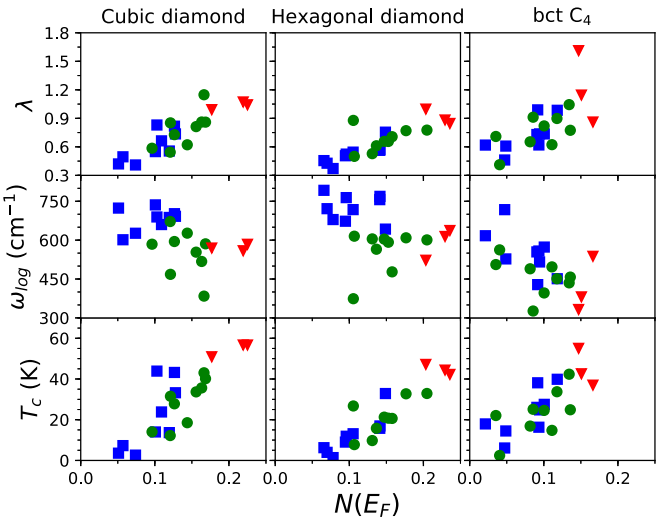

FIG. 4. Superconducting transition temperature (T_c in K, bottom panels), logarithmic average of phonon frequency ($\omega_{\log}$ in cm^{-1}, center panels), and electron-phonon coupling constant (λ, top panels) for three boron-doped carbon materials as a function of electronic DOS at the Fermi energy [$N(E_F)$ in states/eV/atom]. Left, center, and right columns show the results for cubic diamond, hexagonal diamond, and bct C_4, respectively. Blue squares and green circles represent the data for 12.5% and 25% boron-doped cases with boron pairing, respectively. Red triangles represent the results for 25% doping without boron paring.

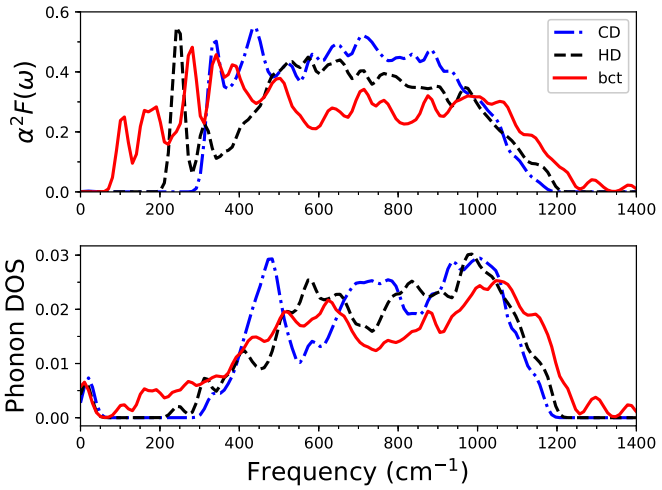

FIG. 5. Eliashberg spectral function (top panel) and phonon density of states (bottom panel) of 25% boron-doped cubic diamond (blue dash-dotted lines), hexagonal diamond (black dashed lines), bct C_4 (red solid lines). Here we select the structure with the highest T_c for each material. The finite phonon DOS around the zero frequency is an artifact because of the unconverged acoustic phonon modes at the Γ point.

weak because of $\omega_{\log}$ dependence. Boron pairing generally eliminates effective carriers at the Fermi energy and results in a relatively low $N(E_F)$ and T_c. Therefore, a uniform boron doping is desirable for achieving high T_c.

In Fig. 4, the slope of the linear relation between $N(E_F)$ and λ is steeper in cubic diamond than in hexagonal diamond. Hexagonal diamond has an anisotropic structure between the plane spanned by a vectors and c directions. The electronic properties also exhibit anisotropy due to this structural anisotropy. The valence-band top at the Γ point is doubly degenerated and the wave functions are distributed in the a plane. However, a similar wave function along the z direction is about 0.5 eV below the valence top states. Such anisotropy in electronic states does not promote electron-phonon coupling when compared with cubic diamond. The maximum of $N(E_F)$ is relatively low for the bct C_4 case because of the localized states created by the emergence of sp^2-hybridized atoms. Nevertheless, the superconducting parameters are comparable to the other materials.

The Eliashberg spectral function and phonon density of states (phonon DOS) of boron-doped systems shown in Fig. 5 describe the characteristic phonon and superconducting properties of each material. Cubic diamond (blue dash-dotted line) exhibits the smallest phonon frequency range (from 300 to 1200 cm^{-1}). This reflects the robustness of cubic diamond as a host material for boron substitutional doping. Hexagonal diamond exhibits low-frequency modes below 300 cm^{-1}. These low-frequency modes arise from relatively long boron-carbon bonds and further softened low-frequency scissor modes. The integrated Eliashberg spectral function up to 500 cm^{-1} is almost the same in cubic diamond and hexagonal diamond. However, the resulting λ is larger in cubic diamond by 0.07 because of the larger contributions from middle-frequency phonon modes (between 600 and 1000 cm^{-1}).

Further low-frequency phonon modes below 200 cm^{-1} appears in bct C_4 (red solid lines in Fig. 5). The low-frequency modes significantly contribute to the Eliashberg spectral function when compared with the other materials. These modes involve collective twisting motion of the four-membered ring. In addition, higher-frequency phonon modes above 1200 cm^{-1} are also observed and contribute to the spectral function and phonon DOS in bct C_4. The low-frequency contribution arises from the collective twisting motion of the four-membered ring. The high-frequency modes are associated with the sp^2-hybridized atoms caused by the boron doping [see Fig. 2(d)]. Interestingly, the contribution from low- and high-frequency modes in bct C_4 is similar to that of amorphous carbon where large empty space also exists in its structure [20,21]. The high T_c of 55 K in this structure suggests that perfect symmetry of the crystal structure or perfect tetrahedra are not necessarily required to obtain such a high T_c.

The structure with the highest T_c for each material is further studied with a combination of a $6 \times 6 \times 6$ k grid and $2 \times 2 \times 2$ q grid to confirm the q dependence. The difference in T_c is approximately 10% in all three cases, as listed in Table III. We also consider a few different structures other than those listed here, but the errors are even smaller and always less than 10%. These results confirm that increasing the q grid to $2 \times 2 \times 2$ does not significantly affect the calculated superconducting properties when we use these sizes of supercells.

IV. SUMMARY

In summary, we study structural, electronic, and superconducting properties of substitutional boron-doped cubic diamond, hexagonal diamond, and bct C_4. The key structural character for high T_c is the absence of boron pairing inside carbon materials. Cubic and hexagonal diamond exhibit similar trends because of their structural similarity. The characteristic structure in bct C_4 is the origin of the distinct responses to boron doping. It is interesting that even boron-doped bct C_4 could exhibit superconductivity around 50 K despite its considerable structural distortion. If heavy boron doping in

TABLE III. Superconducting parameters of 25% boron-doped cubic diamond, hexagonal diamond, and bct C_4 with the highest T_c for each material. The two subcolumns show the results with the Γ-only sampling and $2 \times 2 \times 2 \times$ q grid for electron-phonon calculations.

	Cubic diamond		Hexagonal diamond		bct C_4	
	Γ	$2 \times 2 \times 2$	Γ	$2 \times 2 \times 2$	Γ	$2 \times 2 \times 2$
λ	1.07	1.25	1.00	1.00	1.61	1.42
$\omega_{\log}$	804	707	752	694	478	495
T_c	56.7	61.9	47.2	43.8	55.0	50.2

bct C_4 is achieved, the boron pairing should be avoided as the boron pairing costs high energy. The upper bound of T_c is around 60 K in cubic diamond. A higher boron concentration than 25% does not significantly contribute to the $N(E_F)$. A further high T_c in boron-doped amorphous carbon suggested in the literature [39] requires a different mechanism for superconductivity as the $N(E_F)$ does not increase with an excess amount of boron doping.

ACKNOWLEDGMENTS

Y.S. and J.R.C. acknowledge support from the U.S. Department of Energy (DOE) for work on nanostructures from Grant No. DE-FG02-06ER46286, and on algorithms by a subaward from the Center for Computational Study of Excited-State Phenomena in Energy Materials at the Lawrence Berkeley National Laboratory, which is funded by the U.S. Department of Energy, Office of Science, Basic Energy Sciences, Materials Sciences and Engineering Division under Contract No. DEAC02-05CH11231, as part of the Computational Materials Sciences Program. Computational resources are provided in part by the National Energy Research Scientific Computing Center (NERSC). M.L.C. acknowledges the National Science Foundation Grant No. DMR-1926004 support for research associated with conceptualizing and developing the theory and from the Theory of Materials Program at the Lawrence Berkeley National Laboratory funded by the Director, Office of Science and Office of Basic Energy Sciences, Materials Sciences and Engineering Division, U.S. Department of Energy under Contract No. DE-AC02-05CH11231 for supporting research related to the computational aspects involved in this project.

[1] K. S. Novoselov, A. K. Geim, S. V. Morozov, D. Jiang, Y. Zhang, S. V. Dubonos, I. V. Grigorieva, and A. A. Firsov, Science **306**, 666 (2004).
[2] S. Iijima, Nature (London) **354**, 56 (1991).
[3] N. Hamada, S.-i. Sawada, and A. Oshiyama, Phys. Rev. Lett. **68**, 1579 (1992).
[4] H. W. Kroto, J. R. Heath, S. C. O'Brien, and R. E. Smalley, Nature (London) **318**, 162 (1985).
[5] Y. Chen, Y. Y. Sun, H. Wang, D. West, Y. Xie, J. Zhong, V. Meunier, M. L. Cohen, and S. B. Zhang, Phys. Rev. Lett. **113**, 085501 (2014).
[6] Y. Sakai, S. Saito, and M. L. Cohen, Phys. Rev. B **91**, 165434 (2015).
[7] P. A. Schultz, K. Leung, and E. B. Stechel, Phys. Rev. B **59**, 733 (1999).
[8] Q. Li, Y. Ma, A. R. Oganov, H. Wang, H. Wang, Y. Xu, T. Cui, H.-K. Mao, and G. Zou, Phys. Rev. Lett. **102**, 175506 (2009).
[9] K. Umemoto, R. M. Wentzcovitch, S. Saito, and T. Miyake, Phys. Rev. Lett. **104**, 125504 (2010).
[10] J.-T. Wang, C. Chen, and Y. Kawazoe, Phys. Rev. Lett. **106**, 075501 (2011).
[11] K. Tanigaki, T. W. Ebbesen, S. Saito, J. Mizuki, J. S. Tsai, Y. Kubo, and S. Kuroshima, Nature (London) **352**, 222 (1991).
[12] T. E. Weller, M. Ellerby, S. S. Saxena, R. P. Smith, and N. T. Skipper, Nat. Phys. **1**, 39 (2005).
[13] N. Murata, J. Haruyama, J. Reppert, A. M. Rao, T. Koretsune, S. Saito, Y. Matsudaira, and M. Yagi, Phys. Rev. Lett. **101**, 027002 (2008).
[14] J. Haruyama, M. Matsudaira, J. Reppert, A. Rao, T. Koretsune, S. Saito, H. Sano, and Y. Iye, J. Supercond. Nov. Magn. **24**, 111 (2011).
[15] E. A. Ekimov, V. A. Sidorov, E. D. Bauer, N. N. Mel'nik, N. J. Curro, J. D. Thompson, and S. M. Stishov, Nature (London) **428**, 542 (2004).
[16] Y. Takano, T. Takenouchi, S. Ishii, S. Ueda, T. Okutsu, I. Sakaguchi, H. Umezawa, H. Kawarada, and M. Tachiki, Diamond Relat. Mater. **16**, 911 (2007).
[17] H. Okazaki, T. Wakita, T. Muro, T. Nakamura, Y. Muraoka, T. Yokoya, S. Kurihara, H. Kawarada, and T. Oguchi, Appl. Phys. Lett. **106**, 052601 (2015).
[18] Y. Cao, V. Fatemi, S. Fang, K. Watanabe, T. Taniguchi, E. Kaxiras, and P. Jarillo-Herrero, Nature (London) **556**, 43 (2018).
[19] A. Bhaumik, R. Sachan, and J. Narayan, ACS Nano **11**, 5351 (2017).
[20] Y. Sakai, J. R. Chelikowsky, and M. L. Cohen, Phys. Rev. B **97**, 054501 (2018).
[21] Y. Sakai, J. R. Chelikowsky, and M. L. Cohen, Phys. Rev. Mater. **3**, 084802 (2019).
[22] A. Bhaumik and J. Narayan, Nanoscale **11**, 9141 (2019).
[23] J. Narayan and A. Bhaumik, J. Appl. Phys. **118**, 215303 (2015).
[24] Y. Sakai, J. R. Chelikowsky, and M. L. Cohen, Phys. Rev. Mater. **2**, 074403 (2018).
[25] J. E. Moussa and M. L. Cohen, Phys. Rev. B **77**, 064518 (2008).
[26] J. Ihm, A. Zunger, and M. L. Cohen, J. Phys. C **12**, 4409 (1979).
[27] M. L. Cohen, Phys. Scr. **T1**, 5 (1982).
[28] P. Hohenberg and W. Kohn, Phys. Rev. **136**, B864 (1964).
[29] W. Kohn and L. J. Sham, Phys. Rev. **140**, A1133 (1965).
[30] P. Giannozzi, S. Baroni, N. Bonini, M. Calandra, R. Car, C. Cavazzoni, D. Ceresoli, G. L. Chiarotti, M. Cococcioni, I. Dabo, A. Dal Corso, S. de Gironcoli, S. Fabris, G. Fratesi, R. Gebauer, U. Gerstmann, C. Gougoussis, A. Kokalj, M. Lazzeri, L. Martin-Samos, N. Marzari, F. Mauri, R. Mazzarello, S. Paolini, A. Pasquarello, L. Paulatto, C. Sbraccia, S. Scandolo, G. Sclauzero, A. P. Seitsonen, A. Smogunov, P. Umari, and R. M. Wentzcovitch, J. Phys. Condens. Matter **21**, 395502 (2009).
[31] N. Troullier and J. L. Martins, Phys. Rev. B **43**, 1993 (1991).
[32] D. M. Ceperley and B. J. Alder, Phys. Rev. Lett. **45**, 566 (1980).
[33] J. P. Perdew and A. Zunger, Phys. Rev. B **23**, 5048 (1981).
[34] S. Baroni, S. de Gironcoli, A. dal Corso, and P. Giannozzi, Rev. Mod. Phys. **73**, 515 (2001).
[35] F. Giustino, Rev. Mod. Phys. **89**, 015003 (2017).
[36] P. B. Allen and R. C. Dynes, Phys. Rev. B **12**, 905 (1975).
[37] J. P. Goss and P. R. Briddon, Phys. Rev. B **73**, 085204 (2006).
[38] M. Parrinello and A. Rahman, Phys. Rev. Lett. **45**, 1196 (1980).
[39] J. Nayaran, R. Sachan, and A. Bhaumik, Mater. Res. Lett. **7**, 164 (2019).